*Pharmaceutical Research, Vol. 27, No. 3, March 2010 (© 2010)*
DOI: 10.1007/s11095-009-0036-7

*Research Paper*

# Leakiness and Size Exclusion of Paracellular Channels in Cultured Epithelial Cell Monolayers–Interlaboratory Comparison

**Alex Avdeef**[1,2]

*Received September 23, 2009; accepted December 10, 2009; published online January 13, 2010*

***Purpose.*** To determine and compare the paracellular characteristics of permeability ($P_{app}$) of Caco-2, MDCK, and 2/4/A1 cell lines.
***Methods.*** The $P_{app}$ data from 14 studies were analyzed by weighted nonlinear regression in terms of the paracellular parameters: porosity-pathlength (ε/δ), pore radius (R), and electrostatic potential drop ($\Delta\varphi$). Aqueous diffusivities, $D_{aq}$, for the analysis, were empirically determined. The required hydrodynamic radii, $r_{HYD}$, were estimated without knowledge of compound density. Mannitol iso-paracellular profiles allowed comparisons of "leakiness" across labs.
***Results.*** $D_{aq}$ (37°C) was predicted as $9.9\times10^{-5}$ $MW^{-0.453}$; $r_{HYD}=(0.92+21.8\ MW^{-1})\cdot r_{SE}$, where $r_{SE}$ is the Stokes-Einstein radius. Values of pore radius ranged from 4.0(±0.1) to 18(±3) Å, with the 2/4/A1 indicating the largest pores. The ε/δ capacity factor ranged from 0.2 (±0.1) to 69 (±5) $cm^{-1}$, with most values <1.5 $cm^{-1}$. The average potential drop for Caco-2 models was $\Delta\varphi_{wt\ avg}^{Caco\text{-}2}=-43\pm20$ mV. The paracellular model predicted measured log $P_{app}$ values with pooled $r^2=0.93$ and $s=0.17$ ($n=108$).
***Conclusion.*** R and ε/δ are negatively correlated to a large extent. $P_{app}$ can be rate-limited by either factor, with a wide range of possible combinations still indicating nearly constant leakiness for a given marker.

**KEY WORDS:** 2/4/A1 cell line; Caco-2; paracellular permeability; interlaboratory comparison; MDCK.

## INTRODUCTION

The epithelial cell monolayer is an integral part of the inner lining of the intestine, in direct contact with the passing luminal fluid. The individual cells are held together by a complex of proteins that circumscribe the cells near the luminal surface (1). Diamond (2) described the epithelium akin to a "six-pack of beer," with each can representing a barrel-shaped epithelial cell and the plastic holder ring ("flannister") encircling each cell at the top side, holding the cells together. The bottoms of the cans represent the baso-lateral membranes, which face the blood stream in the neighboring basal capillaries. The flannister, in this cartoon, represents the tight junction barrier complex.

The tight junction forms an important protective barrier in the gastrointestinal tract (GIT) that regulates the paracellular diffusion of small polar molecules and ions through size-restricted water-filled channels between the cells, but excludes potentially toxic large molecules and microbes. The ease with which small solvated ions, such as $Na^+$ and $Cl^-$, can move through these channels can be estimated by the transepithelial electrical resistance (TEER) (2). The human stomach surface is usually classed as "tight," with a 2,000 Ω.$cm^2$ TEER value; the small intestine is thought to be "leaky," indicated by 50–100 Ω.$cm^2$; the colonic TEER is "intermediate" in tightness, with 300–400 Ω.$cm^2$ values (3). Usually, the surface area assumed in the intestinal resistance measurement is based on the "smooth cylinder" model (4,5). However, the fold and villus structures in the small intestine can effectively expand the available surface area by up to 30 times (4–9), and if this were taken into account, the intestinal TEER values could more closely match those of the stomach, given the smoother gastric surface (4–11).

The understanding of paracellular transport has been derived mainly from the study of *in vitro* cultured cell models, such as the Caco-2 and MDCK (Madin-Darby Canine Kidney) immortalized cell lines (10,12–21). A very leaky cell line, 2/4/A1, was studied by Tavelin *et al.* (18), as a possible model to represent the human small intestine. The restrictiveness of the paracellular junction to the permeation of small hydrophilic drug-like solutes depends on the number of paracellular channels per unit area of surface, the size of the pores in the channels, and the charged residues lining the channels (2) (e.g., negatively charged groups, some being carboxylic acid residues, characterized by a $pK_a$ of about 4.5). The charge gives rise to cation selectivity. For example, junctional conductance of $Na^+$ increases with pH from 3 to 6, while that of $Cl^-$ decreases (2). The effective porosity, ε, of

Contribution number 27 in the *PAMPA—a Drug Absorption in vitro Model* series from *p*ION. Ref. 26 is part 26 in the series.

**Electronic supplementary material** The online version of this article (doi:10.1007/s11095-009-0036-7) contains supplementary material, which is available to authorized users.

[1] pION INC, 5 Constitution Way, Woburn, Massachusetts 01801, USA.
[2] To whom correspondence should be addressed. (e-mail: aavdeef@pion-inc.com)

the epithelium depends on the area of exposed aqueous channels intercalating the cells in relation to the total surface area of cells exposed to the lumen. Estimates range from $10^{-3}$ to $10^{-5}$ for ε (3,10). Using an effusion theory approach, Linnankoski *et al.* (22) estimated ε to be between $2.4\times10^{-7}$ (MDCK) and $1.5\times10^{-6}$ (2/4/A1). Small cells (e.g., those lining the crypt of the intestinal barrier structure) have larger fractions of available paracellular channels than larger cells (e.g., those lining the villus tips of the intestinal wall) (11). A capacity factor may be defined as the ratio of ε to δ, the rate-limiting paracellular junction pathlength. Common values of the capacity factor ε/δ are ~ 1 $cm^{-1}$. In the various *in vitro* cellular models, reported values of the pore radius, R, range from 3.7 Å (18) to 12–15 Å (13,22), with a value near 6 Å thought to be characteristic of tight junctions (13–19). There are many discussions in the literature of the magnitude of R, but few of the capacity factor, ε/δ.

Adson *et al.* (13) were the first to characterize quantitatively the leakiness and size exclusion properties of the paracellular junctions in Caco-2 monolayers in terms of all three parameters: ε/δ, R, and Δφ. They judiciously selected nine marker molecules, including positively and negatively charged solutes, spanning a wide range of sizes. Their computational procedure involved selecting pairs of marker molecules to extract R from the ratio of their apparent permeability coefficients. From the average value of $R$=12 Å, they calculated the capacity factor, ε/δ=1.22 $cm^{-1}$. Pade and Stavchansky (15) reported a ε/δ value of 0.267 $cm^{-1}$. Values for the human intestine have not been reported. From the enhancement/attenuation of permeability of the cationic/anionic species, in relation to that of the neutral molecules, the average potential drop, Δφ=−17.7 mV, was determined by these investigators in their landmark study.

In the published analyses of the junction parameters, molecular radii, r, are sometimes calculated from molar volumes (when the densities of the compounds are available). Aqueous diffusivities, $D_{aq}$, are then calculated from r, using the Stokes-Einstein (SE) equation: $D_{aq}=k_BT / (6\pi\,\eta\,r)$, where $k_B$ = Boltzmann constant, T = absolute temperature, and η = kinematic viscosity of the solvent. Implicit in this association is that $D_{aq}$ is proportional to the inverse cube root of molecular weight. However, for small drug-like molecules (<1,000 Da), $D_{aq}$ is more accurately predicted as a function of inverse square root of molecular weight (21,23,24). The SE equation works well for large and nearly-spherical macromolecules, but becomes less predictive for molecules with solute size less than five times that of the solvent (25). The Sutherland (Su) equation (25) is thought to be better suited for small spherical molecules; the factor 6 in the SE equation is replaced with 4 in the Su equation.

We were interested to re-examine the earlier analyses of the paracellular parameters and to compare results from different laboratories by using an empirically derived relationship between $D_{aq}$ and MW (21,24) and by using a modified Stokes-Einstein equation to estimate hydrodynamic radii, where the denominator coefficient "6" is set to be a function of MW, taking on values between 6 (SE) and 4 (Su). In the course of the study, we developed a more general mathematical procedure for determining ε/δ, R, and Δφ, and other related paracellular parameters, and applied it to the *in vitro* epithelial cell permeability data from 14 different studies (12–21). Preliminary results of this analysis, based on the data of Adson *et al.* (13), were used in an "in combo" PAMPA model developed to predict the absorption properties of 33 ampholytes (mostly zwitterions) (26). Here, we present the first *interlaboratory* analysis of the leakiness and size exclusion properties of three different epithelial cell models (Caco-2, MDCK, and 2/4/A1) (12–21).

## COMPUTATIONAL METHOD

### Aqueous Diffusivity Equation Derived from Measured Data

The aqueous diffusivity data at 25°C were collected from standard tabulations (25,27,28), Flynn *et al.* (23), and sources containing measured data for drug molecules (29,30). The 160 compounds with MW<1,200 Da (cf., Supplemental Table) were analyzed using linear regression, as had been done by us earlier for 87 molecules (21). The analysis tested the dependent variables log $D_{aq}$ as a function of the independent variables, log MW and log $P_{OCT}$ (octanol-water partition coefficient):

$$\log D_{aq} = A + B \log MW + C \log P_{OCT} \tag{1}$$

where $A$, $B$, and $C$ are multi-linear regression coefficients. The rationale for including log $P_{OCT}$ stemmed from the tendency of lipophilic molecules to form aggregates in solution, with markedly attenuated diffusivity.

### Paracellular Pore Radius, Porosity, and Electric Gradient Analysis

The apparent (measured) permeability of a cellular monolayer encompasses three permeability contributions: (a) aqueous boundary layer ($P_{ABL}$), (b) transcellular ($P_{trans}$), and (c) paracellular ($P_{para}$), according to the well-tested equation (10)

$$\frac{1}{P_{app}} = \frac{1}{P_{ABL}} + \frac{1}{P_{trans} + P_{para}} \tag{2}$$

$P_{ABL}$ represents the resistance of the stagnant water layer adjacent to the cellular monolayer surface, and is related to the aqueous diffusivity ($D_{aq}$) of the permeant and the thickness of the boundary layer ($h_{ABL}$) according to the simple expression

$$P_{ABL} = \frac{D_{aq}}{h_{ABL}} \tag{3}$$

Here, $D_{aq}$ ($cm^2\ s^{-1}$) values were empirically determined, using Eq. 1. The factor 1.339 was used to convert $D_{aq}$ values from 25 to 37°C. The thickness of the boundary layer, $h_{ABL}$, depends on the rate of stirring in the *in vitro* permeability assay, with typical values being about 1,000–4,000 μm in unstirred solutions and about 500 μm in solutions efficiently stirred at 50 RPM (rev $min^{-1}$) (21,24).

The transcellular permeability, $P_{trans}$, represents the permeation of the apical and basolateral bilayer membranes of the cells. In the absence of carrier-mediated or active transport, the transcellular permeability can be well-modeled by PAMPA measurements (21). To a lesser degree of precision, the octanol-water partition coefficient, measured at pH 7.4 as log $D_{OCT}$, can

be a suitable substitute. To determine the $P_{trans}$ contribution of paracellular marker molecules to the apparent permeability, $P_{app}$, we chose to use log $D_{OCT}$ here, since for many of the marker molecules (e.g., mannitol, methylamine, urea, acetic acid, etc.), reliable PAMPA values are not available. In the permeability model, it was assumed that

$$\log P_{trans} = a + b \log D_{OCT} \tag{4}$$

where $a$ and $b$ are empirical parameters determined by regression analysis of $P_{app}$ data, and log $D_{OCT}$ values were calculated at pH 7.4 using the measured $pK_a$ values and the measured log $P_{OCT}$, taken from the literature (13,24,31).

From the solution to the differential flux equation describing size-restricted diffusion through a cylindrical channel containing charged groups, under sink boundary condition, the paracellular permeability, $P_{para}$, can be expressed as (10,13)

$$P_{para} = \left(\frac{\varepsilon}{\delta}\right) \cdot D_{aq} \cdot F\left(\frac{r}{R}\right) \cdot E(\Delta\varphi) \tag{5}$$

The ε/δ capacity factor represents the porosity-pathlength ratio, where the porosity is the relative surface area of the junction opening divided by the total epithelial surface area, and the pathlength, δ, represents the thickness of the restricted-junction domain times the tortuosity of the water channels. In the study here, no differentiation was made between the tight-junction and the lateral-space (10) contributions to the paracellular resistance, so the refined ε/δ may be viewed as an "apparent" porosity-pathlength ratio.

F(r/R) is the Renkin (32) hydrodynamic sieving function for cylindrical water channels, defined as

$$F\left(\frac{r}{R}\right) = \left[1 - \left(\frac{r}{R}\right)\right]^2 \cdot \left[1 - 2.104\left(\frac{r}{R}\right) + 2.09\left(\frac{r}{R}\right)^3 - 0.95\left(\frac{r}{R}\right)^5\right] \tag{6}$$

The junction pore radius is denoted as R (Å).

The hydrodynamic radius, r (Å), can be estimated from the Stokes-Einstein large spherical-particle equation:

$$r_{SE} = \frac{k_B T}{6\pi \eta D_{aq}} \tag{7a}$$

provided the aqueous diffusivity is known; or it can be estimated by the less-commonly cited Sutherland equation (25):

$$r_{Su} = \frac{k_B T}{4\pi \eta D_{aq}} \tag{7b}$$

which is more appropriate than the Stokes-Einstein equation when small molecules are considered (25); or the Glasstone equation, which has the factor 2π (in place of 4 π and 6π) and is thought to better match some experimental results (25); or the molecular radius can be estimated from the molar volume (not requiring knowledge of $D_{aq}$), as was done by Adson *et al.* (13):

$$r_{MV} = \sqrt[3]{\frac{3MW}{4\pi\rho N_A}} \tag{7c}$$

where η is the kinematic viscosity (0.006962 $cm^2\ s^{-1}$ at 37°C), ρ is the compound density (g $cm^{-3}$), $N_A$ is the Avagadro number, and the other terms have their usual meaning. (For the usual choice of units, Eqs. 7a–7c need to be multiplied by $10^{+8}$ to convert from cm to Å.) It is not convenient to use Eq. 7c for research compounds, since the compound density is usually not known. On the other hand, Eqs. 7a and 7b can be generally applied, since diffusivity can be estimated from MW, according to Eq. 1. The compound density values for most of the paracellular markers considered here are readily available. This allowed us to compare the various different estimates of the hydrodynamic radii. In the present study, we expected that for very large molecules, Eq. 7a would be most suitable, but for very small molecules, Eq. 7b would be most suitable. The largest paracellular marker in the Adson study, $Phe_3Gly$ (516.6 Da), indicates $r_{SE}/r_{MV}$=5.59/5.46 = 1.03, while the smallest marker, methylamine (31.1 Da), indicates $r_{SE}/r_{MV}$= 1.56/2.60 = 0.60; these ratios approximately match the 6:4 relationship between the SE and Su equations. A fit of $r_{SE}/r_{MV}$ *vs.* MW allowed us to define the scaling factor, g, whose value ranges from about 4 to 6, in the equation developed here:

$$r_{HYD} = \frac{k_B T}{g \cdot \pi \eta D_{aq}} \tag{7d}$$

The E(Δφ) term in Eq. 5 is a function of the potential drop across the electric field created by negatively charged residues lining the junctional pores, and can be defined as (10)

$$E(\Delta\varphi) = f_{(0)} + f_{(+)} \cdot \frac{\kappa \cdot |\Delta\phi|}{1 - e^{-\kappa \cdot |\Delta\phi|}} + f_{(-)} \cdot \frac{\kappa \cdot |\Delta\phi|}{e^{+\kappa \cdot |\Delta\phi|} - 1} \tag{8}$$

where $f_{(o)}$, $f_{(+)}$, and $f_{(-)}$ are the concentration fractions of the molecule in the uncharged, cationic, and anionic forms, respectively (where $f_{(o)}+f_{(+)}+f_{(-)}$ =1). The potential drop across the electric gradient is denoted by Δφ. The constant, $\kappa=(F / N_A k_B T)=0.037414\ mV^{-1}$ at 37°C, where $F$ is the Faraday constant, and other symbols have their usual meaning. A potential drop, Δφ, of −17.7 mV was estimated by Adson *et al.* (13) for their Caco-2 model. Accordingly, a negatively charged molecule would have E(Δφ)=0.7, and a positively charged drug would have E(Δφ)=1.4.

## Refinement of the Paracellular Parameters

The *p*CEL-X v2.0 program (*p*ION) was used to determine the $a$, $b$, ε/δ, R, and Δφ parameters by a nonlinear weighted regression analysis. The regression equation was constructed from Eqs. 2–8:

$$G = \log\left(\frac{1}{P_{app}^{Caco-2}} - \frac{h_{ABL}}{D_{aq}}\right) = -\log\left[a \cdot D_{OCT}^{b} + \frac{\varepsilon}{\delta} \cdot D_{aq} \cdot F\left(\frac{r_{HYD}}{R}\right) \cdot E(\Delta\phi)\right] \tag{9}$$

The partial derivatives of G with respect to $a$, $b$, ε/δ, R, and Δφ were calculated explicitly in the *p*CEL-X program, using standard mathematical techniques. The function minimized was

$$S = \sum_i^n \left(\frac{G_i^{obs} - G_i^{calc}}{\sigma_i(\log P_{app})}\right)^2 \tag{10}$$

where n is the number of paracellular marker molecules used in the model, and $\sigma_i(\log P_{eff})$ is the reported standard deviation of the logarithm of the $i^{th}$ measured Caco-2 permeability corresponding to the markers. The effectiveness of the simultaneous refinement of $n_V$ parameters was characterized by the "goodness-of-fit," GOF = $[S/(n\text{-}n_V)]^{1/2}$, which has the expectation value of 1 if the model is suitable for the data and the measured standard deviations accurately reflect the precision of the data.

### Selection Criteria for Paracellular Permeability Data from Various Laboratories

Due to the focus of the study, marker molecules chosen for paracellular analysis from the various published studies were compounds likely not to have significant transcellular component in the transport, so that Eq. 4 would only play a minor corrective role (since the accuracy of predicting $P_{trans}$ from $D_{OCT}$ is expected to be limited). With two borderline exceptions, all compounds were characterized by log $D_{OCT}$< 0. The marker selection task in three publications (12–14) was made easy, since the investigators specifically selected molecules to characterize the paracellular mechanism. In the more general source studies, we looked for a wide range in sizes of marker molecules, preferring urea (found in 9 of 14 studies) at the low end and mannitol (in 8 of 14 studies) at the high end. In some selected studies, small charged solutes were characterized as well, including methylamine (13,14) and acetate (13). The Garberg *et al*. (20) study considered several epithelial cell lines with the same set of compounds and contained information on carrier-mediated transport, such as that of lactic acid, alanine, L-DOPA, and α-Me-DOPA. Also, Caco-2 cells are known to express enzymes such as sucrase, that can hydrolyze sucrose and other disaccharides, as noted by Garberg *et al*. (20). The MDCK $P_{app}$ of sucrose in the study averaged $0.3\times10^{-6}$ cm $s^{-1}$, whereas the Caco-2 $P_{app}$ indicated (20) an average value about three times higher, but the standard deviation was also high (cf., Fig. 3h). In this one instance, the sucrose Caco-2 value was used in our study. As another example, the glycerol Caco-2 (but not MDCK) absorptive (apical-to-basolateral) $P_{app}$ was about six times higher than the excretive $P_{app}$, suggesting the possibility of a facilitated uptake mechanism. That value was excluded in our study. Thus, only compounds, which were not knowingly substrates of transporters based upon the literature, were chosen for the final analysis.

As a point of nomenclature in the cited papers, the MDCK cell lines were called simply "MDCK" from American Type Culture Collection (13,20), "MDCK mdr-1" (transfected mdr-1 gene) (20), and "MDCK wt" (wild type, untransfected version) (20), the latter two originating from The Netherlands Cancer Institute. Table I lists the marker molecules considered in the 14 selected studies, reported in eight different publications (12–14,16–20).

## RESULTS AND DISCUSSION

### Analysis of Aqueous Diffusivity

Fig. 1 shows a plot of the log $D_{aq}$ *vs.* log MW for 160 drug-like and other simple (mostly neutral) molecules, ranging in MW from 30 to 1,200 Da. (The Supplementary Data contains the list of compounds used.) All of the data are normalized to 25°C. The symbols in filled circles are compounds with log $P_{OCT}$<3. The unfilled circles are associated with compounds with 3<log $P_{OCT}$<4, and the checkered symbols are of compounds with log $P_{OCT}$>4. The data were tested by linear regression, using Eq. 1, but the improvement in the quality of the fit was minimal with the inclusion of the log $P_{OCT}$. The compounds with log $P_{OCT}$>4 ultimately were assigned zero weights, on the concern that possible aggregates may have formed with some of the steroidal derivatives in the group.

The analysis of compounds with log $P_{OCT}$<4 produced the empirical relationship ($r^2$=0.94, $s$=0.04, $n$=147):

$$\log D_{aq} = -4.13 - 0.453 \log MW \tag{11}$$

The two coefficients are nearly the same as those published previously, albeit then using about half the number of compounds in the correlation analysis (21). Table I lists the $D_{aq}$ values for paracellular markers calculated with the above equation.

### Analysis of the Hydrodynamic Radius of Drugs

To calculate molecular radii using Eq. 7c, it is necessary to know compound density. Adson *et al.* (13) reported the densities of their paracellular markers (although some values may have been estimates—e.g., atenolol and the peptides). Additional values were collected from numerous sources. For a few markers whose density values were not found, ACD/ChemSketch (v3.0) from Advanced Chemistry Development (Toronto, Canada) was used to calculate the missing values. Table I lists the density values used. Also listed are the estimated molecular radii, $r_{SE}$, based on the Stokes-Einstein relationship (Eq. 7a), and values of $r_{MV}$, calculated based on the molar volume, according to Eq. 7c. Fig. 2 shows a plot of $r_{SE}/r_{MV}$ *vs.* MW for the marker molecules in Table I. The data were fitted to a hyperbolic function, from which we deduced the g-factor for the Sutherland-Stokes-Einstein relationship, Eq. 7d.

$$r_{HYD} = \frac{k_B T}{\left(\frac{6.52MW}{MW+23.7}\right)\cdot \pi\,\eta\, D_{aq}} = \left(0.92 + \frac{21.8}{MW}\right)\cdot r_{SE} \tag{12}$$

$D_{aq}$ in the above equation was derived from Eq. 11. The $r_{HYD}$ then were used in the Renkin function (Eq. 6) in all subsequent analysis of the paracellular parameters. A linear regression analysis of the relationship between the diffusivity-based and the molar volume-based radii produces the relationship: $r_{MV}$=−0.16(±0.21)+1.06(±0.05) $r_{HYD}$ ($r^2$=0.92, $s$=0.25, $F$=426, $n$=38). Hence, $r_{HYD}$ is a useful estimate of $r_{MV}$ in the absence of density data, which may be helpful particularly with research compounds.

### Paracellular Analysis

#### *Refined Paracellular Parameters*

Fig. 3 shows the paracellular analysis results for eleven of the fourteen studies considered here. The preliminary Caco-2

**Table I.** Data for the Marker Compounds Used in the Paracellular Analysis[a]

| COMPOUND | MW | log $D_{OCT}$ | $D_{aq}$ ($10^{-6}$ cm $s^{-1}$) | ρ (g $cm^{-3}$) | $r_{SE}$ (Å) | $r_{MV}$ (Å) | $r_{HYD}$ (Å) | %para |
|---|---|---|---|---|---|---|---|---|
| NEUTRAL | | | | | | | | |
| urea | 60.1 | −1.66 | 15.5 | 1.32 | 2.11 | 2.62 | 2.71 | 90–98 |
| glycerol | 92.1 | −1.76 | 12.7 | 1.25 | 2.56 | 3.08 | 2.96 | 95–98 |
| creatinine | 113.1 | −1.77 | 11.6 | 1.37 | 2.81 | 3.20 | 3.13 | 90–96 |
| erythritol | 122.1 | −2.29 | 11.2 | 1.32 | 2.91 | 3.32 | 3.20 | 97 |
| alanine | 89.1 | −2.96 | 12.9 | 1.42 | 2.52 | 2.92 | 2.94 | 99 |
| mannitol | 182.2 | −3.10 | 9.4 | 1.52 | 3.49 | 3.62 | 3.63 | 91–99 |
| L-DOPA | 197.2 | −2.76 | 9.0 | *1.47* | 3.61 | 3.76 | 3.72 | 99 |
| a-ME-DOPA | 211.2 | −2.27 | 8.8 | *1.40* | 3.73 | 3.91 | 3.81 | 94 |
| acyclovir | 225.2 | −1.81 | 8.5 | *1.77* | 3.84 | 3.69 | 3.90 | 88–92 |
| D-Phe-Gly | 222.2 | −2.16 | 8.6 | 1.24 | 3.82 | 4.14 | 3.88 | 96 |
| cimetidine | 252.3 | 0.35 | 8.1 | 1.31 | 4.04 | 4.24 | 4.07 | 29–69 |
| hydrochlorothiazide | 297.7 | −0.05 | 7.5 | *1.69* | 4.36 | 4.12 | 4.33 | 19–67 |
| lactulose | 342.3 | −3.59 | 7.0 | 1.32 | 4.64 | 4.68 | 4.56 | 93 |
| sucrose | 342.3 | −3.65 | 7.0 | 1.29 | 4.64 | 4.72 | 4.56 | 96–99 |
| raffinose | 504.4 | −8.09 | 5.9 | 1.59 | 5.53 | 5.01 | 5.33 | 95–100 |
| POSITIVE | | | | | | | | |
| methylamine | 31.1 | −3.86 | 20.9 | 0.70 | 1.56 | 2.60 | 2.54 | 74–96 |
| terbutaline | 225.3 | −1.37 | 8.5 | *1.17* | 3.84 | 4.24 | 3.90 | 87 |
| atenolol | 266.3 | −1.92 | 7.9 | 1.13 | 4.14 | 4.54 | 4.15 | 92–97 |
| ranitidine | 314.4 | 0.32 | 7.3 | *1.18* | 4.47 | 4.72 | 4.42 | 18–71 |
| sulpiride | 341.4 | −0.42 | 7.0 | 1.34 | 4.64 | 4.66 | 4.56 | 59–91 |
| NEGATIVE | | | | | | | | |
| formate | 46.0 | −4.18 | 17.5 | 1.22 | 1.87 | 2.46 | 2.61 | 97 |
| acetate | 60.1 | −3.18 | 15.5 | 1.05 | 2.11 | 2.83 | 2.71 | 98 |
| lactate | 90.1 | −4.36 | 12.9 | 1.36 | 2.53 | 2.97 | 2.94 | 98–100 |
| foscarnet | 126.0 | −6.13 | 11.1 | *2.14* | 2.95 | 2.86 | 3.22 | 96–100 |
| hippurate | 179.2 | −3.44 | 9.4 | 1.37 | 3.46 | 3.73 | 3.60 | 98 |
| clodronate | 244.9 | −4.14 | 8.2 | *2.31* | 3.99 | 3.48 | 4.02 | 85–97 |
| chlorothiazide | 295.7 | −0.51 | 7.5 | *2.04* | 4.34 | 3.86 | 4.32 | 23–70 |
| furosemide | 330.8 | −1.17 | 7.1 | *1.61* | 4.57 | 4.34 | 4.50 | 57 |
| D-Phe-Phe-Gly | 369.4 | −1.46 | 6.8 | *1.26* | 4.80 | 4.88 | 4.70 | 85 |
| D-Phe-Phe-Phe-Gly | 516.6 | −0.66 | 5.8 | *1.26* | 5.59 | 5.46 | 5.38 | 56 |
| PROPYLENE GLYCOLS | | | | | | | | |
| PEG194 | 194.2 | −3.00 | 9.1 | *1.11* | 3.59 | 4.11 | 3.71 | 86 |
| PEG238 | 238.3 | −4.48 | 8.3 | *1.11* | 3.94 | 4.39 | 3.98 | 96 |
| PEG282 | 282.3 | −4.47 | 7.7 | *1.11* | 4.25 | 4.65 | 4.24 | 97 |
| PEG326 | 326.4 | −4.46 | 7.2 | *1.11* | 4.54 | 4.88 | 4.48 | 99 |
| PEG370 | 370.4 | −4.45 | 6.8 | *1.12* | 4.81 | 5.09 | 4.71 | 99 |
| PEG414 | 414.5 | −4.44 | 6.4 | *1.12* | 5.06 | 5.28 | 4.92 | 100 |
| PEG458 | 458.5 | −4.43 | 6.2 | *1.12* | 5.30 | 5.46 | 5.13 | 100 |
| PEG502 | 502.6 | −4.80 | 5.9 | *1.12* | 5.52 | 5.63 | 5.32 | 100 |

[a] $D_{aq}$ calculated by Eq. 11. The density, ρ, values in italics are calculated values (ACD/ChemSketch Rev. 3.0, Advanced Chemistry Development, Toronto, Canada). The molecular radii $r_{SE}$, $r_{MV}$, and $r_{HYD}$ were calculated with Eqs. 7a, 7c, and 12, respectively. %para represents the fraction of the transport that involves the paracellular junction route.

re-analysis of the Adson *et al.* (13) data are presented elsewhere (26). The frames in Fig. 3 are arranged in the increasing order of the estimated pore radius, R. Lower values of R are indicated by higher slopes in the plot of log $P_{app}$–log $D_{aq}$. (The inclusion of $D_{aq}$ helps to normalize the plots for ordinate changes due to molecular weight.) The solid best-fit curve is associated with the uncharged markers (cf., Table I). These curves were calculated as the product of refined parameters: $\varepsilon/\delta \cdot F(r_{HYD}/R)$ (cf., Eqs. 5 and 6, with $E(\Delta\varphi)=1$). In the studies that included cationic and anionic solutes, the best-fit curves for the charged solutes are indicated by plus and minus symbol curves, respectively. The actual measured points may not necessarily lie on the curves, even when the data are well-fitted, if the molecules are transported appreciably by the transcellular route. Table I summarizes the ranges of percentage of transport due to the paracellular mode, as "%para," for each of the markers studied. It's clear that some compounds indicated significant percentage of transcellular contribution (e.g., ranitidine, hydrochlorothiazide, and cimetidine in some of the studies). Modeling $P_{trans}$ with the octanol-water partition coefficient has a long history, e.g., early efforts by Levin *et al.* (31), who reported the coefficient $b=0.56$ for Eq. 4. The value we used was fixed at $b=0.54$, based on our own correlation comparisons between Caco-2 $P_{app}$ and log $D_{OCT}$ (data not shown). It was not possible to refine both *a* and *b* in Eq. 4, based on the paracellular marker data. In fact, only in two of the 14 sets (Table II) was it possible to refine the value of a, since most of the markers were dominantly paracellular in character.

Table II summarizes the results of the paracellular model refinement using the interlaboratory epithelial cell data and the regression design Eq. 9. The pore radius ranged from 4.0 (±0.1)

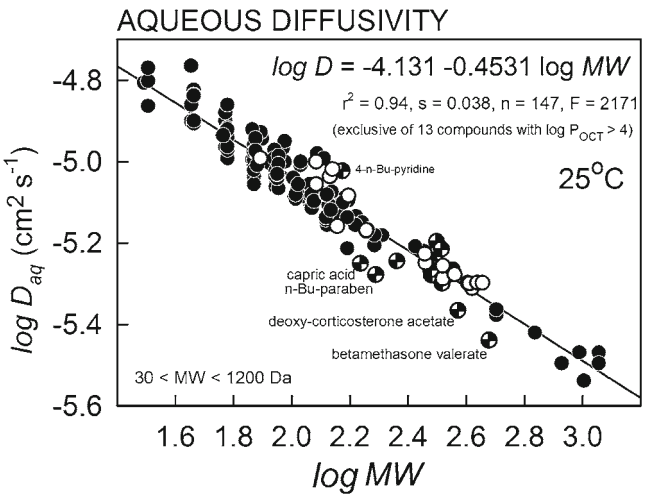


**Fig. 1.** Correlation plot of aqueous diffusivity (normalized to 25°C) *vs.* molecular weight, as log $D_{aq}$ *vs.* log MW, for 160 drug-like and other simple (mostly neutral) molecules. Filled circles: compounds with log $P_{OCT}$<3; unfilled circles: 3<log $P_{OCT}$<4; checkered symbols: compounds with log $P_{OCT}$>4.

to 18(±3) Å, with the high end associated with the leaky 2/4/A1 line developed in the Artursson laboratory (18) and the low end (Caco-2) also originating from the same laboratory. The ε/δ capacity factor spanned a larger range of values, from 0.2 (±0.1) $cm^{-1}$ for the MDCK (ATCC) data of Garberg *et al.* (20) to 69 (±5) $cm^{-1}$ for the MDCK data of Adson *et al.* (13), reflecting an unexpected 345-fold range in capacity. Half of the values of ε/δ in Table II were 1.5 $cm^{-1}$ or lower.

The potential drops across the junctions for Caco-2 cells ranged from −15 to −82 mV, but the uncertainty in the determination was greater than that of the other two parameters. The weighted average value for Caco-2 models was $\Delta\varphi_{wt\ avg}{}^{Caco\text{-}2}$=−43±20 mV. Only two results based on the MDCK cells were obtained ($\Delta\varphi_{wt\ avg}{}^{MDCK}$=−104±56 mV), but these evaluations can only be viewed as tentative, since the MDCK sampling was so small and the relative errors so high. The 2/4/A1 cell line indicated only a very minimal electrical potential effect.

The parameters for Eq. 4 were generally set at $a$=−6.40 and $b$=0.54, and were not refined. However, in two cases, it was possible to refine the former parameter as −6.40±0.31 for the Adson data (13) and −6.36±0.33 for the Alsenz and Haenel data (19).

Fig. 3 indicates the apparent deviations of measured $P_{app}$ data (corrected for diffusivity) from the predicted curves, some deviations appearing substantial. In part, this is because Fig. 3 does not separate out the effects of transcellular component of transport. The 14 individual lab/cell line refinement results were actually quite good, with data points agreeing with calculation to within an average of 2.4 standard deviations (cf., GOF values in Table II). Fig. 4 shows these individual-treatment residuals collated from all 14 calculations. This is not a global calculation that may suggest an over-fitting of the data.

### *Iso-paracellular Profiles*

Since each of the laboratories whose data were used here had somewhat different paracellular markers, and since the protocols used to prepare the cell lines differed from lab to lab, it was challenging to compare the ε/δ and R between different groups. As is evident in Table II, the lowest four pore radii (4.0–5.4 Å) were nearly the same, suggesting comparable "leakiness." But the apparent leakiness varied substantially due to the seven-fold variation in the capacity factors (10–69 $cm^{-1}$), seemingly not depending on the pore radii. Furthermore, the capacity factors for these tightest junction cases were substantially larger than those cases associated with larger pore radii (R>6 Å), which were characterized by ε/δ<6 $cm^{-1}$. Comparing "leakiness" was not so straight-forward, although there appeared to be an inverse relationship between the capacity factor and the pore radius.

Consistent with the above collations, but not evident from any discussions in the published literature, was that the simultaneous refinement of ε/δ and R parameters indicated very extensive negative correlation, with correlation coefficients often above 90%. Nonetheless, the generally high quality of the published *in vitro* data allowed for determination of the individual parameters, with relatively good precision in many instances (Table II).

A method to compare the relative "leakiness" of the various cell lines was developed in this study. Mannitol was selected as a standard paracellular marker for the leakiness scale. It was assumed that it is possible to have a wide range of ε/δ and R (correlated) parameters such that the paracellular permeability of mannitol would be the same for each pair over a range of value combinations. Fig. 5 illustrates this concept. The vertical axis is a plot of log (ε/δ), and the horizontal axis is the pore radius. The analyzed ε/δ and R parameters are indicated by the symbols: squares for MDCK, circles for Caco-2 and diamond for 2/4/A1 cell lines. Each symbol is associated with a continuous capacity curve, where any position on the curve would have the same value of predicted $P_{app}$ of mannitol. $P_{para}$ of mannitol was calculated according to the refined paracellular parameters (Table II). The capacity curve was then calculated by dividing $P_{para}{}^{mannitol}$ by $D_{aq}{\cdot}F(r_{HYD}/R)$, as suggested by Eq. 5 (E(Δφ) = 1). The capacity curve *vs.* R for a constant paracellular permeability is called the iso-paracellular profile here.

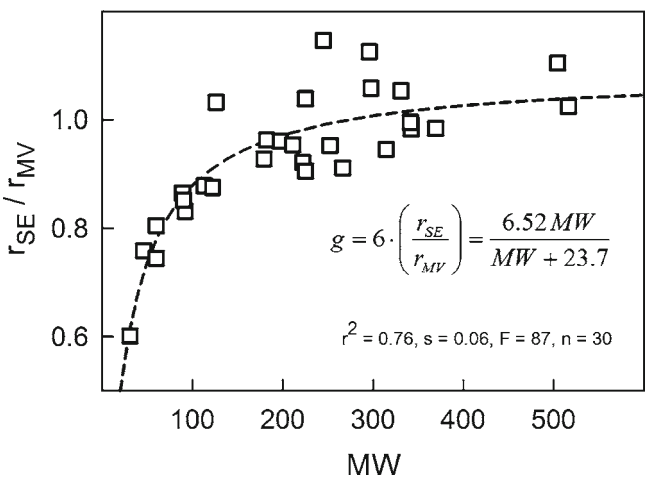


**Fig. 2.** Comparison of the ratios of molecular radii determined from the Stokes-Einstein equation ($r_{SE}$) and molecular volume ($r_{MV}$) to the molecular weight of the paracellular marker molecules in Table I. The $r_{SE}/r_{MV}$ ratios are fitted to a hyperbolic function of molecular weight, MW, to deduce the g-factor (cf., Eq. 7d).

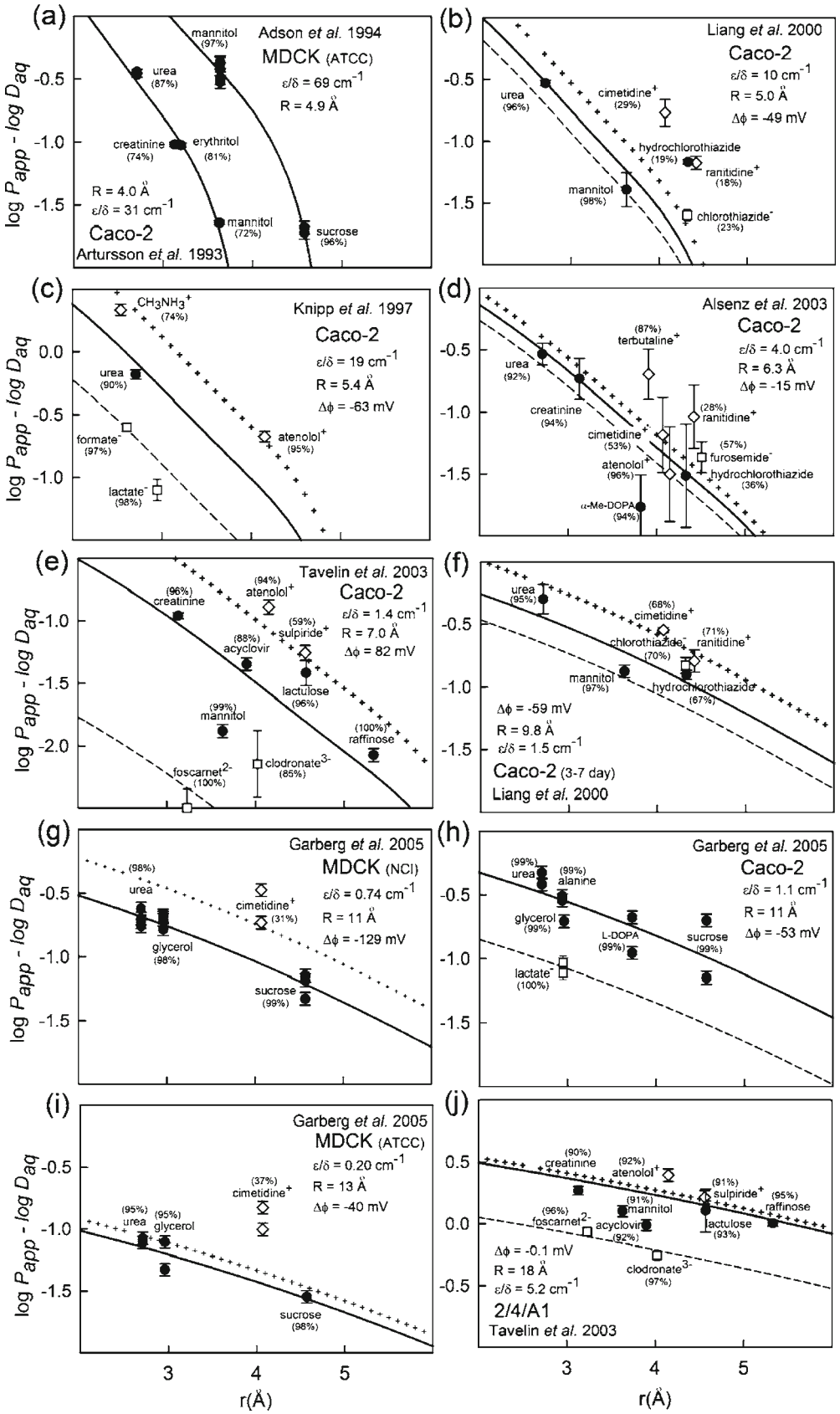


**Fig. 3.** Plot of the Caco-2, MDCK and 2/4/A1 data, as $\log P_{app} - \log D_{aq}$ *vs.* molecular radius, for the paracellular markers selected in this study. The solid line corresponds to the neutral compounds; the "+++" lines correspond to the positively-charged molecules, and the dashed line corresponds to the negatively-charged molecules (see text). Excessive deviations are in part due to transcellular components in the apparent permeability.

**Table II.** Results of Paracellular Analysis[a]

| Cells | Source | (ε/δ) ($cm^{-1}$) | R(Å) | $-\Delta\varphi$ (mV) | GOF | n | $P_{para}$ (urea) | $P_{para}$ (mannitol) | $P_{para}$ (sucrose) | $P_{para}$ (raffinose) | Size Exclusion (urea/sucrose) |
|---|---|---|---|---|---|---|---|---|---|---|---|
| Caco-2 | Artursson *et al.* 1993 | 31 ± 6 | 4.0±0.1 | 30[b] | 4.5 | 5 | 4.7 | 0.19 | 0[c] | 0[c] | >1000 |
| MDCK (25°C) | Adson *et al.* 1994 | 69±5 | 4.9±0.1 | 30[b] | 1.2 | 9 | 30 | 3.5 | 0.15 | 0[c] | 200 |
| Caco-2 | Liang *et al.* 2003 | 10±5 | 5.0±0.3 | 49±107 | 2.6 | 6 | 4.7 | 0.55 | 0.03 | 0[c] | 157 |
| Caco-2 | Knipp *et al.* 1997 | 19±29 | 5.4±1.2 | 63±5 | 1.6 | 6 | 13 | 1.7 | 0.22 | 0[c] | 59 |
| Caco-2 (7 day) | Alsenz & Haenel 2003 | 4±14 | 6.3±3.5 | 15±25 | 1.2 | 9 | 4.9 | 0.83 | 0.17 | 0.04 | 29 |
| Caco-2 | Tavelin *et al.* 2003 | 1.4±4 | 7.0±3.1 | 82±8 | 4.7 | 9 | 2.4 | 0.49 | 0.11 | 0.04 | 22 |
| Caco-2 (3-7 day) | Liang *et al.* 2003 | 1.5±4 | 9.8±4.1 | 59±39 | 2.9 | 6 | 5.5 | 1.8 | 0.63 | 0.27 | 9 |
| MDCK (NCI) | Garberg *et al.* 2005 | 0.74±0.2 | 10.7±0.7 | 129±41 | 1.5 | 14 | 3.2 | 1.1 | 0.43 | 0.20 | 7 |
| Caco-2 | Garberg *et al.* 2005 | 1.11±0.9 | 11.1±1.9 | 55±11 | 3.0 | 11 | 5.1 | 1.8 | 0.73 | 0.35 | 7 |
| MDCK (ATCC) | Garberg *et al.* 2005 | 0.20±0.1 | 12.7±1.5 | 40±67 | 1.6 | 8 | 1.1 | 0.43 | 0.19 | 0.10 | 6 |
| Caco-2 (25°C) | Adson *et al.* 1994 | 0.78±0.4 | 12.9±1.6 | 30±3 | 1.4 | 10 | 4.4 | 1.7 | 0.79 | 0.43 | 5 |
| 2/4/A1 | Tavelin *et al.* 2003 | 5.2±3 | 17.8±2.9 | 0.1[b] | 2.8 | 9 | 39 | 18 | 9.9 | 6.3 | 4 |

[a] $P_{para}$ values are predicted for urea, mannitol, sucrose, and raffinose, based on the refined paracellular parameters. Size Exclusion index = Ppara(urea)/Ppara(mannitol). GOF = goodness-of-fit (see text); n = number of $P_{app}$ values refined in the sources study.
[b] Not refined.
[c] Not permeable by paracellular route, since $r_{HYD}$>R.

For example, the (ε/δ, R) values for the Caco-2 data from Knipp *et al.* (14), Liang *et al.* (3–7 day model) (16), Garberg *et al.* (20), and Adson *et al.* (13) are vastly different, yet all four of the sets are positioned essentially on the same iso-paracellular curve (Fig. 5). The leakiness (using mannitol as standard) is nearly identical, even though pore radii range from 5.4 to 12.9 Å. The four sets show different balance of limiting factors: the Knipp data indicate limited permeability due to the small pore radius, whereas the Adson data indicate limited permeability due to the small capacity factor (either shortage of paracellular channels, ε, or especially long paracellular pathlengths, δ).

The ensemble of iso-paracellular curves in Fig. 5 allows the comparative visualization of the relative leakiness of the cell lines and the nature of the leakiness-limiting parameters (pore *vs.* capacity factor). As can be seen, the leakiest cell line is 2/4/A1, and the tightest cell line is that of Caco-2, both developed by Artursson and coworkers (12,18). The MDCK characteristics are broadly equal to those of Caco-2 (Fig. 5).

### *Ranking by Size Exclusion*

Fig. 5 indicates a relative leakiness series based on mannitol. However, if a different standard were chosen, then the ranking of leakiness would be somewhat different. The "size exclusion" ratio, $P_{para}^{urea} / P_{para}^{sucrose}$, is an indication of how sensitive a particular cell line is to changes in the size of solute. The last column in Table II lists the size exclusion ratio for twelve of the cell studies considered. This ratio parallels the ranking by the pore radius. Fig. 6 shows a bar graph of twelve studies, each with the predicted paracellular permeability for four increasingly larger markers: urea, mannitol, sucrose, and raffinose. As can be seen, the rank order of leakiness depends on the specific marker used, although in all cases of comparison, 2/4/A1 ranks as the leakiest.

### *Propylene Glycol Oligomers as Markers for Paracellular Permeability*

When we included PEGs in the data to characterize the paracellular parameters, the PEG compounds indicated

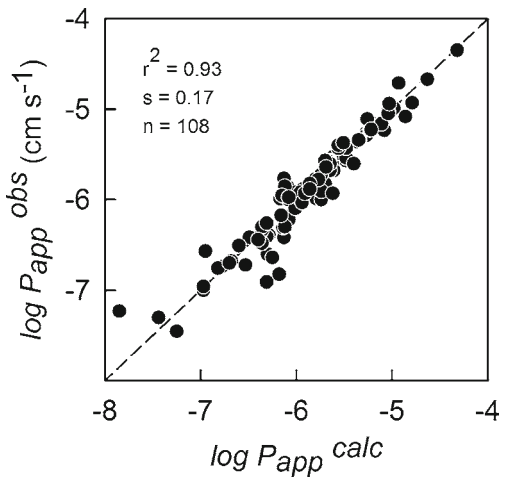


**Fig. 4.** Pooled statistics of observed and calculated log $P_{app}$, based on the regression model according to Eq. 9.

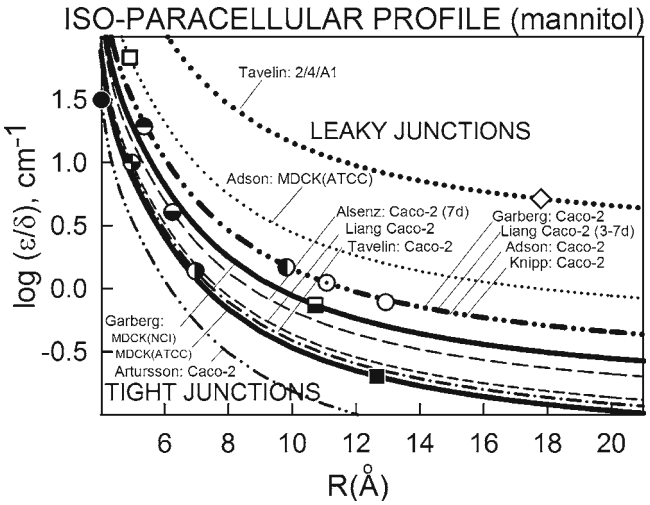


**Fig. 5.** Iso-paracellular profiles: log (ε/δ) *vs.* the pore radius, R, at constant $P_{app}$. The determined [log (ε/δ), R] values are squares for MDCK, circles for Caco-2 and diamond for 2/4/A1 cell lines. Each symbol is associated with a continuous capacity curve, where any position on the curve would correspond to the same value of predicted $P_{app}$ of mannitol. The capacity curves were calculated as $P_{para} \cdot D_{aq}^{-1} \cdot F(r_{HYD}/R)^{-1}$, using mannitol as the standard marker.

"anomalous" characteristics. This had been noted in the past in two critical studies: Artursson *et al.* (12) and Watson *et al.* (17), where oligomers ranging from 194 Da to 502 Da were individually characterized. Artursson and coworkers proposed that PEGs may be able to permeate the channels more easily than other molecules used as paracellular markers, due to their highly non-spherical shapes, perhaps diffusing with decreased resistance due to the smaller axial cross section. Watson and coworkers proposed an explanation for the increased permeability of PEGs, compared to other drug-like markers, on the grounds that the known (33) hydrodynamic radii of the PEGs are nearly 1 Å less than those calculated by Eq. 7c.

A new analysis of the permeability of PEG homologues (282–898 Da) in Caco-2, MDCK, 2/4/A1 cell lines, as well as excised human jejunal patches, was recently reported by Linnankoski *et al.* (22) They applied the effusion theory-based equation to estimate the porosities (ε) and pore sizes (R) of the membranes. In MDCK and Caco-2 cells, the paracellular route for the PEG homologues was best interpreted by a two-pore model, with the smaller pores being 5.5–5.8 Å, and the larger pores being 10.4–30.5 Å. It is interesting that the 2/4/A1 cells indicated a single-pore behavior, with $R$=14.9 Å, an estimate which is larger than the previously determined value of 9 Å (18). The 2/4/A1 R value in our study, 17.8±2.9 Å, agrees reasonably well with that of Linnankoski *et al.* (22). The effusion-equation-determined porosities rank for PEG homologues as MDCK<Caco-2<2/4/A1 < human jejunal patch. For the MDCK cells (22), $\varepsilon = 2.4 \times 10^{-7}$. If the ε/δ determined from the data of Garber *et al.* (20) (0.20 and 0.74 $cm^{-1}$, Table II) is combined with the effusion-based ε, the paracellular rate-limiting pathlength, δ, would be predicted to be between 3 and 12 nm. The latter range appears to be less than that determined from histological studies, 100–250 nm (3,10).

Since both the *in situ* human jejunal perfusion permeability ($P_{eff}$) and the human bioavailability (%F) have been reported for many of the PEG homologues (34–36), it was interesting to compare the %F *vs.* log $P_{eff}$ plot of PEGs to that of the 31 drug compounds reviewed by Lennernäs (37). Apparently, there is a clean break between the drug and the PEG curves, with PEGs showing about a 10-fold higher permeability for a given level of bioavailability (Avdeef A and Tam KY, submitted).

The use of PEGs as paracellular markers is clearly complicated, somewhat controversial, and deserves further investigation.

## CONCLUSION

The interlaboratory comparison of the leakiness and size exclusion of fourteen cultured epithelial cell monolayer models (Caco-2, MDCK, 2/4/A1) has shown that the ranking by relative leakiness depends on the choice of the paracellular standard compound, since leakiness can be limited either by the capacity factor or the pore radius, two parameters that are substantially inversely correlated. With $D_{aq}(37°C) = 9.9 \times 10^{-5} MW^{-0.453}$ and $r_{HYD} = (0.92 + 21.8\ MW^{-1}) \cdot r_{SE}$ in the weighted nonlinear regression analysis, values of pore radius were determined to be 4.0(±0.1) to 18(±3) Å and the ε/δ capacity factor to be 0.2 (±0.1) to 69 (±5) $cm^{-1}$; the potential drop for Caco-2 models was $\Delta\varphi_{wt\text{-}avg}^{Caco\text{-}2} = -43 \pm 20$ mV. This was the first unified treatment of the paracellular parameters characterizing the properties of cultured cell lines from

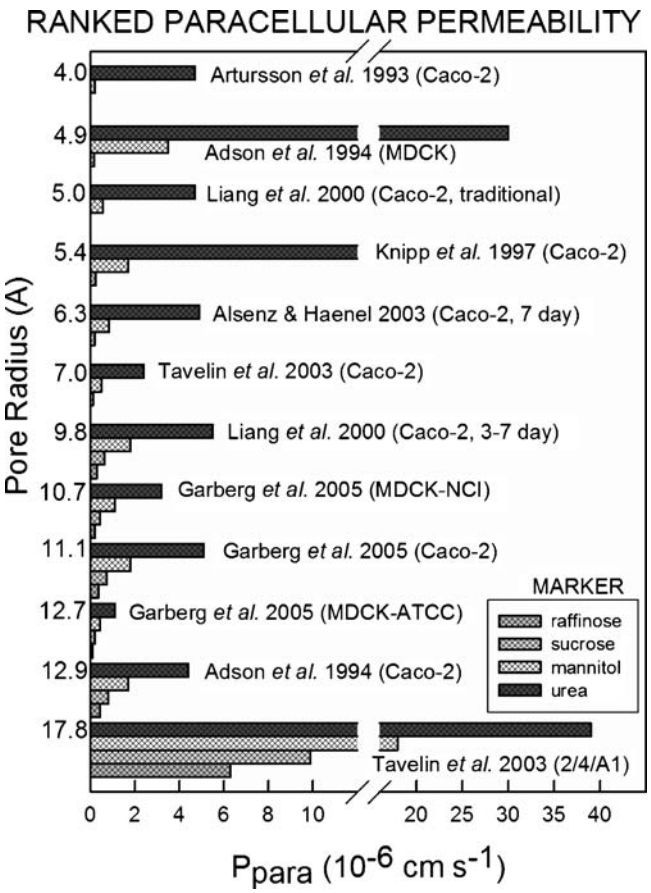


**Fig. 6.** Ranking paracellular permeability of four markers (urea, mannitol, sucrose, raffinose) according to increasing junction pore radius.

different laboratories, and may serve as a model for characterizing newly established cell lines or for monitoring the constancy of established epithelial cell lines.

## ACKNOWLEDGEMENT

Helpful discussions with Dr. Kin Y. Tam (AstraZeneca, UK) and Dr. Kiyohiko Sugano (Pfizer, UK) are gratefully acknowledged. The long-term guiding influence of Prof. Norman F. H. Ho is deeply appreciated.

## REFERENCES

1. Farquhar MG, Palade GE. Junctional complexes in various epithelia. J Cell Biol. 1963;17:375–412.
2. Diamond JM. The epithelial junction: bridge, gate, and fence. Physiologist. 1977;20:10–8.
3. Fleisher D. Biological transport phenomena in the gastrointestinal tract: cellular mechanisms. In: Amidon GL, Lee PI, Topp EM, editors. Transport processes in pharmaceutical systems. New York: Marcel Dekker, Inc; 2000. p. 147–84.
4. Oliver RE, Jones AF, Rowland M. What surface of the intestinal epithelium is effectively available to permeating drugs? J Pharm Sci. 1998;87:634–9.
5. Sugano K. Introduction to computational oral absorption simulation. Expert Opin Drug Metab Toxicol. 2009;5:259–93.
6. Wilson JP. Surface area of the small intestine in man. Gut. 1967;8:618–21.
7. Moog F. The lining of the small intestine. Sci Amer. 1981;245 (11):154–76.
8. Pappenheimer JR. Scaling of dimensions of small intestines in non-ruminant eutherian mammals and its significance for absorptive mechanisms. Compar Biochem Physiol A. 1998;121:45–58.
9. Desesso JM, Williams AL. Contrasting the gastrointestinal tracts of mammals: factors that influence absorption. Annual Rep Med Chem. 2008;43:353–71.
10. Ho NFH, Raub TJ, Burton PS, Barsuhn CL, Adson A, Audus KL, *et al.* Quantitative approaches to delineate passive transport mechanisms in cell culture monolayers. In: Amidon GL, Lee PI, Topp EM, editors. Transport processes in pharmaceutical systems. New York: Marcel Dekker; 2000. p. 219–316.
11. Madara JL. Functional morphology of the small intestine. In: Schultz SG, editors. Handbook of Physiology, Sec. 6: The Gastrointestinal System, Am. Physiol. Soc.: Bethesda; 1991. p. 92.
12. Artursson P, Ungell A-L, Löfroth J-E. Selective paracellular permeability in two models of intestinal absorption: cultured monolayers of human intestinal epithelial cells and rat intestinal segments. Pharm Res. 1993;10:1123–9.
13. Adson A, Raub TJ, Burton PS, Barsuhn CL, Hilgers AR, Audus KL, *et al.* Quantitative approaches to delineate paracellular diffusion in cultured epithelial cell monolayers. J Pharm Sci. 1994;83:1529–36.
14. Knipp GT, Ho NFH, Barsuhn CL, Borchardt RT. Paracellular diffusion in Caco-2 cell monolayers: effect of perturbation on the transport of hydrophilic compounds that vary in charge and size. J Pharm Sci. 1997;86:1105–10.
15. Pade V, Stavchansky S. Estimation of the relative contributions of the transcellular and paracellular pathway to the transport of passively absorbed drugs in the Caco-2 cell culture model. Pharm Res. 1997;14:1210–5.
16. Liang E, Chessic K, Yazdanian M. Evaluation of an accelerated Caco-2 cell permeability model. J Pharm Sci. 2000;89:336–45.
17. Watson CJ, Rowland M, Warhurst G. Functional modeling of tight junctions in intestinal cell monolayers using polyethylene glycol oligomers. Am J Physiol Cell Physiol. 2001;281:C388–97.
18. Tavelin S, Taipalensuu J, Söderber L, Morrison R, Chong S, Artursson P. Prediction of oral absorption of low-permeability drugs using small intestine-like 2/4/A1 cell monolayers. Pharm Res. 2003;20:397–405.
19. Alsenz J, Haenel E. Development of a 7-day, 96-well Caco-2 permeability assay with high throughput direct UV compound analysis. Pharm Res. 2003;20:1961–9.
20. Garberg P, Ball M, Borg N, Cecchelli R, Fenart L, Hurst RD, et al. *In vitro* models for the blood-brain barrier. Toxicol *In Vitro*. 2009;19:299–334.
21. Avdeef A, Artursson P, Neuhoff S, Lazarova L, Gråsjö J, Tavelin S. Caco-2 permeability of weakly basic drugs predicted with the Double-Sink PAMPA $pK_a^{flux}$ method. Eur J Pharm Sci. 2005;24:333–49.
22. Linnankoski J, Mäkelä J, Palmgren J, Mauriala T, Vedin C, Ungell A-L, Lazorova L, Artursson P, Urtti A, Yliperttula M. Paracellular porosity and pore size of the human intestinal epithelium in tissue and cell culture models. J Pharm Sci. 2009; (Epub ahead of print: doi:10.1002/jps.21961).
23. Flynn GL, Yalkowsky SH, Roseman TJ. Mass transport phenomena and models: theoretical concepts. J Pharm Sci. 1974; 63:479–510.
24. Avdeef A. Absorption and drug development. New York: Wiley-Interscience; 2003. p. 207–8.
25. Cussler EL. Diffusion—mass transfer in fluid systems. 2nd ed. Cambridge: Cambridge University Press; 1997. p. 111–21.
26. Tam KY, Avdeef A, Tsinman O, Sun N. The permeation of amphoteric drugs through artificial membranes—an *in combo* absorption model based on paracellular and transmembrane permeability. J Med Chem. 2009;(Epub ahead of print: doi:10.1021/jm901421c).
27. Weast RC, Astle MJ, editors. CRC handbook of chemistry and physics. 60th ed. Boca Raton: CRC; 1979–1980. p. F-62.
28. Lide DR, editor. CRC handbook of chemistry and physics. 78th ed. Boca Raton: CRC; 1997–1998. p. 5.94–5.
29. Seki T, Mochida J, Okamoto M, Hosoya O, Juni K, Morimoto K. Measurement of diffusion coefficients of parabens and steroids in water and 1-octanol. Chem Pharm Bull. 2003;51:734–6.
30. Amidon GE, Higuchi WI, Ho NFH. Theoretical and experimental studies of transport of micelle-solubilized solutes. J Pharm Sci. 1982;71:77–84.
31. Levin VA, Dolginow D, Landahl HD, Yorke C, Csejtey J. Relationship of octanol/water partition coefficient and molecular weight to cellular permeability and partitioning in S49 lymphoma cells. Pharm Res. 1984;1:259–66.
32. Renkin EM. Filtration, diffusion and molecular sieving through porous cellulose membranes. J Gen Physiol. 1954;38:225–38.
33. Ruddy SB, Hadzija BW. Iontophoretic permeability of polyethylene glycols through hairless rat skin: application of hydrodynamic theory for hindered transport through liquid-filled pores. Drug Des Discov. 1992;8:207–24.
34. Chadwick VS, Phillips SF, Hofmann AF. Measurements of intestinal permeability using low molecular weight polyethylene glycols (PEG 400). II. Application to normal and abnormal permeability states in man and animals. Gastroenterology. 1977; 73:247–51.
35. Soderholm JD, Olaison G, Kald A, Tagesson C, Sjodahl R. Absorption profiles for polyethylene glycols after regional perfusion and oral load in healthy humans. Digest Dis Sci. 1997;42:853–7.
36. Maxton DG, Bjarnason I, Reynolds AP, Catt SD, Peters TJ, Menzies IS. Lactulose, $^{51}$Cr-labeled ethylenediaminetetracetate, L-rhamnose and polyethylene glycol 400 as probe markers for assessment *in vivo* of human intestinal permeability. Clin Sci. 1998;71:71–80.
37. Lennernäs H. Intestinal permeability and its relevance for absorption and elimination. Xenobiotica. 2007;37:1015–51.